Deformation-induced splitting of the isoscalar $E0$ giant resonance: Skyrme random-phase-approximation analysis

J. Kvasil,[1] V. O. Nesterenko,[2,*] A. Repko,[1,3] W. Kleinig,[2] and P.-G. Reinhard[4]
[1]*Institute of Particle and Nuclear Physics, Charles University, CZ-18000 Prague 8, Czech Republic*
[2]*Laboratory of Theoretical Physics, Joint Institute for Nuclear Research, Dubna, Moscow Region, 141980, Russia*
[3]*Institute of Physics, Slovak Academy of Sciences, 84511, Bratislava, Slovakia*
[4]*Institut für Theoretische Physik II, Universität Erlangen, D-91058 Erlangen, Germany*
(Received 3 August 2016; revised manuscript received 20 September 2016; published 2 December 2016)

The deformation-induced splitting of isoscalar giant monopole resonance (ISGMR) is systematically analyzed in a wide range of masses covering medium, rare-earth, actinide, and superheavy axial deformed nuclei. The study is performed within the fully self-consistent quasiparticle random-phase-approximation method based on the Skyrme functional. Two Skyrme forces, one with a large (SV-bas) and one with a small (SkP) nuclear incompressibility, are considered. The calculations confirm earlier results that, because of the deformation-induced $E0$-$E2$ coupling, the isoscalar $E0$ resonance attains a double-peak structure and significant energy upshift. Our results are compared with available analytic estimations. Unlike earlier studies, we get a smaller energy difference between the lower and upper peaks and thus a stronger $E0$-$E2$ coupling. This in turn results in more pumping of $E0$ strength into the lower peak and more pronounced splitting of ISGMR. We also discuss widths of the peaks and their negligible correlation with deformation.

DOI: 10.1103/PhysRevC.94.064302

I. INTRODUCTION

The isoscalar giant monopole resonance (ISGMR) is of fundamental interest because it provides information on the nuclear incompressibility [1]; see early [2] and recent [3–5] reviews. In deformed nuclei, the ISGMR exhibits an additional remarkable feature: It couples strongly with the $K^\pi = 0^+$ branch of the isoscalar giant quadrupole resonance (ISGQR), leading to a double-peak structure (splitting) of the ISGMR strength [2]. In prolate nuclei, the high-energy peak constitutes the basic ISGMR while the low-energy peak is produced by the deformation-induced coupling of monopole ($E0$) and quadrupole ($E2$) strengths. The energy difference between the peaks is larger than the widths of ISGMR and ISGQR [2]. In well-deformed nuclei, both peaks carry significant fractions of the monopole strength. As a result, the deformation-induced splitting of ISGMR can be observed experimentally, as, e.g., in ^{154}Sm [6].

The main features of the $E0$-$E2$ coupling and related splitting of the ISGMR were investigated about 30 years ago, theoretically [7–11] and experimentally [7,12,13]. Various models were used: bare Q-Q interaction [7], adiabatic cranking [8], variational [9], fluid-dynamical [10], and quasiparticle random-phase approximation (QRPA) with an effective interaction [11]. The fluid-dynamical study [10] was especially successful. Being self-consistent and based on a simple Skyrme functional, it provided reasonable numerical results and useful analytical estimates.

The interest on ISGMR in deformed nuclei was revived by (i) the appearance of new experimental data, e.g., for Sm [6,14], Mo [15], and Cd [16,17] isotopes, and (ii) the progress of modern self-consistent mean-field models (relativistic, Skyrme, Gogny) [18,19]. In recent self-consistent QRPA calculations, the ISGMR in deformed Mg [20–23], Si [20], Zr [24], and Nd-Sm [25,26] isotopes as well as in ^{238}U [27] was explored. The results of early studies [8–11] were generally confirmed. The importance of self-consistency was corroborated by showing that a self-consistent treatment leads to a narrowing of the ISGMR splitting and thus to a much better agreement with the experiment. Moreover, the influence of neutron excess on the ISGMR properties was investigated [24] and the combined effect of the nuclear incompressibility K_∞ and isoscalar effective mass m_0^*/m on the ISGMR splitting was scrutinized [26].

In the present paper, we present a systematic Skyrme-RPA analysis of the double-peak structure of the ISGMR in prolate axially deformed nuclei. In extension of previous studies, we cover a wide mass region involving medium (Cd), rare-earth (Nd, Sm, Dy, Er, Yb), actinide (U, No), and superheavy (Fl) nuclei. This allows one to check the main trends and analytical estimations [9,10] for the ISGMR. The analysis goes up to the region of superheavy nuclei where the ISGMR had not yet been inspected.

In addition to this survey of deformation splitting, we briefly discuss some contradictions in experimental data on ISGMR from Research Center for Nuclear Physics (RCNP) at Osaka University [14,16] and Texas A&M University (TAMU) [6]. Both groups use the (α,α') reaction and multipole decomposition analysis (MDA) but get substantially different results for the detailed structure of the ISGMR. For example, in well-deformed ^{154}Sm TAMU data [6] demonstrate a distinctive two-peak structure of ISGMR while RCNP data [14] give only one monopole peak. The discrepancies between TAMU and RCNP data for ISGMR in spherical (Sn, Sm, Pb) and deformed (Sm) nuclei were addressed already in our previous studies [25,28]. Here we continue the discussion using RCNP [16] and TAMU [17] results for Cd isotopes. In [16,17], these

*nester@theor.jinr.ru

isotopes are treated as spherical, thus no deformation splitting of ISGMR is assumed. Following experimental data [29] and our calculations, Cd isotopes have a modest quadrupole deformation. Thus some weak double-peak ISGMR structure might be expected here.

Our calculations are performed within the self-consistent QRPA method [30] based on the Skyrme energy functional and specified for axially deformed nuclei [31]. To pin down the $E0$-$E2$ coupling, the self-consistent *separable* random-phase approximation (SRPA) model with Skyrme forces is used [32,33]. In both cases, the pairing is treated within the Bardeen-Cooper-Schrieffer (BCS) scheme [34].

The paper is organized as follows. In Sec. II, the calculation details are outlined. In Sec. III, the results for ISGMR strength functions are discussed. It is demonstrated that just the $E0$-$E2$ coupling is responsible for the double-peak structure of ISGMR. In Sec. IV, the trends for various characteristics of ISGMR are analyzed and compared with analytical estimations. In Sec. V, conclusions are given.

II. CALCULATION SCHEME

The calculations are performed within a two-dimensional (2D) QRPA approach [31]. The method is fully self-consistent because (i) both the mean field and residual interaction are obtained from the same Skyrme functional, (ii) the residual interaction includes all the terms of the initial Skyrme functional as well as the Coulomb direct and exchange terms (the latter in the local-density approximation). Both time-even and time-odd densities are taken into account.

The QRPA code employs a mesh in cylindrical coordinates. The calculation box reaches three nuclear radii. The mesh size is 0.4 fm for medium and rare-earth nuclei, 0.7 fm for U and No and 1.0 fm for superheavy Fl. The single-particle spectrum implements all the levels from the bottom of the potential well up to +30 MeV. Pairing with a contact δ-force interaction (also called volume pairing) is treated at the BCS level [34]. The pairing particle-particle channel is taken into account in the residual interaction.

The ISGMR and ISGQR are computed in terms of $E0$ and $E2$ strength functions:

$$S_0(E\lambda; E) = \sum_\nu |\langle\nu|\hat{M}(E\lambda)|0\rangle|^2\, \xi_\Delta(E - E_\nu), \qquad (1)$$

where $\hat{M}(E0) = \sum_i^A (r^2 Y_{00})_i$ and $\hat{M}(E2) = \sum_i^A (r^2 Y_{20})_i$ are isoscalar ($T = 0$) transition operators, $|0\rangle$ is the ground-state wave function, $|\nu\rangle$ and E_ν are QRPA states and energies. The strength functions include a Lorentz folding with $\xi_\Delta(E - E_\nu) = \Delta/(2\pi[(E - E_\nu)^2 + \Delta^2/4])$ and a folding width Δ. The Lorentz function approximately simulates smoothing effects beyond QRPA (coupling to complex configurations and escape widths) and so allows comparison of calculated and experimental strengths. In the present study, an averaging of $\Delta = 2$ MeV is found optimal. The same folding width was used in the previous studies of the ISGMR [25,26,28].

Two Skyrme forces, SV-bas [35] and SkP, with δ-force pairing [36] are used. Their key properties are characterized by nuclear matter parameters given in Table I. It is seen that these two forces essentially differ by their incompressibilities.

TABLE I. The key parameters of symmetric nuclear matter (incompressibility K_∞, effective mass m_0^*/m, symmetry energy J, slope of symmetry energy L, TRK sum-rule enhancement $\kappa_{\rm TRK}$) for the two Skyrme parametrizations used in this paper.

	K_∞ (MeV)	m_0^*/m	J (MeV)	L (MeV)	$\kappa_{\rm TRK}$
SV-bas	234	0.9	30	32	0.40
SkP	202	1.0	30	20	0.35

The QRPA calculations employ a large configuration space with particle-hole (two-quasiparticle) energies up to 70–75 MeV. Depending on the nucleus, the space involves 8500–9700 configurations with $K = 0$. The spurious mode lies below 2–3 MeV, i.e., safely beyond the ISGMR structures located at 9–20 MeV. For SV-bas, the monopole strength summed in the relevant energy interval 9–45 MeV exhausts the energy weighted sum rule EWSR $= \hbar^2/(2\pi\,\mathrm{m})A\langle \mathrm{r}^2\rangle_0$ by 100%–105%. A similar result is obtained for SkP.

At one place, the quasiparticle separable RPA model (SRPA) [32,33] is also used. SRPA exploits a self-consistent factorization of the residual interaction, which drastically reduces the computational expense while keeping high accuracy of the calculations. The method was successfully applied for description of ISGMR in spherical [28] and deformed [25] nuclei. Here we employ SRPA for analyzing purposes because this model can switch deliberately the $E0$-$E2$ coupling [25] and so allows one to scrutinize the deformation effect in the splitting of the ISGMR. We use in SRPA the same calculational parameters [two-dimensional (2D) cylindrical mesh, size of the configuration space, etc.] as in QRPA.

The QRPA calculations are performed for 24 nuclei from medium, rare-earth, actinide, and superheavy regions. Mainly well-deformed nuclei are considered. The particular isotopic chains (Cd, Nd, Er, No, Fl) are involved. Some chains (Nd, Fl) cover a transition from spherical to deformed nuclei.

For all nuclei, with the exception of Cd isotopes, the equilibrium axial quadrupole deformation β is determined by minimization of the total energy of the system. For soft Cd isotopes, our calculations give shallow energy surfaces with very weak minima. Thus for the Cd chain we use experimental deformation parameters [29].

III. RESULTS AND DISCUSSION

We first consider the ISGMR strength functions which allow a direct inspection of the deformation-induced splitting of the resonance. The low-energy peak appearing from $E0$-$E2$ coupling and high-energy (main) peak tending to the ISGMR in the spherical limit will be discussed.

In Fig. 1, the double-peak structure of ISGMR is illustrated for the case of Nd isotopes. Considered are spherical ^{142}Nd, slightly deformed ^{146}Nd, and well-deformed ^{150}Nd. The low-energy peak in the $E0$ strength grows with deformation. It is absent in spherical ^{142}Nd and significant in strongly deformed ^{150}Nd where the double-peak structure of the ISGMR becomes obvious. The energy of the low-energy peak precisely matches the position of the $K = 0$ branch of the ISGQR (lower panels).

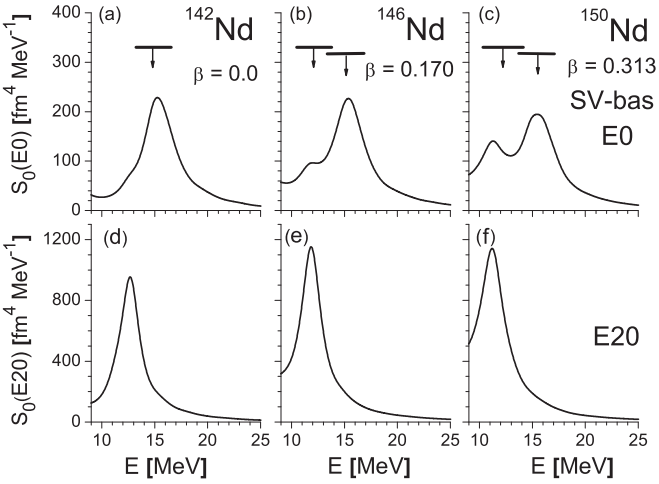

FIG. 1. ISGMR (top panels) and ISGQR($K = 0$) (bottom panels) strength functions in ^{142,146,150}Nd, calculated within QRPA. The calculated deformation parameters are indicated for each isotope. The experimental data (energy centroids and widths) [13] are shown by arrows and horizontal bars.

This indicates that the low-energy peak in the $E0$ strength is caused by the deformation-induced $E0$-$E2$ coupling between ISGMR and ISGQR.

The splitting of the ISGMR strength is further demonstrated in Fig. 2 for well-deformed ^{154}Sm. This example is especially interesting because for ^{154}Sm two sets of experimental data, RCNP [14] and TAMU [6], are available. For convenience of the comparison, we converted the TAMU data [6] given in fractions of the EWSR to units fm^4 MeV^{-1} used in RCNP [14]. In the upper panels, the monopole strength from SRPA calculated without the $E0$-$E2$ coupling is shown (note that,

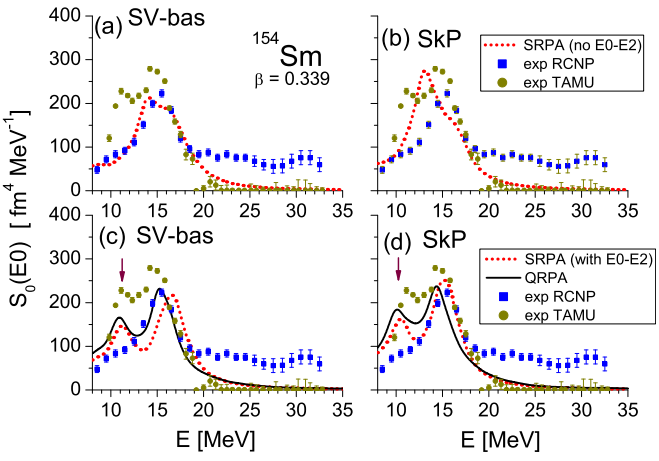

FIG. 2. Isoscalar $E0$ strength functions in deformed ^{154}Sm calculated within SRPA (red dotted lines) and QRPA (black solid lines) with the forces SV-bas (left) and SkP (right). The SRPA calculations are performed without (top panels) and with (bottom panels) the $E0$-$E2$ coupling. For the comparison, the $E0$ data from RCNP [14] (blue filled squares) and TAMU [6] (green filled circles) experiments are depicted. In bottom panels, the calculated peak energies of the $\lambda\mu = 20$ branch of ISGQR are marked by arrows.

unlike QRPA, SRPA allows one to suppress the $E0$-$E2$ coupling in deformed nuclei by skipping the quadrupole terms in the input generators [33]). In this case, the ISGMR, despite the strong deformation, does not exhibit any distinctive double-peak structure but instead comes as one broad peak with some fine structure. However, if we take into account the $E0$-$E2$ coupling (bottom plots), then an additional low-energy peak appears and ISGMR attains a double-peak structure. Moreover, the energy of the low-energy peak coincides with the energy of ISGQR($K = 0$) resonance (marked in the plots by arrows). This takes place in both QRPA and SRPA calculations with Skyrme parametrizations SV-bas and SkP. So Fig. 2 once more proves that just $E0$-$E2$ coupling causes the double-peak structure of ISGMR.

The lower panels of Fig. 2 also show that QRPA calculations with SV-bas correctly reproduce the measured energies of ISGMR peaks, while the calculations with SkP underestimate them. So the incompressibility of SV-bas $K_\infty = 234$ MeV is more reasonable for ^{154}Sm than the SkP value $K_\infty = 202$ MeV. It is worth mentioning that the $K_\infty = 234$ of SV-bas is in accordance with a good reproduction of ISGMR in ^{208}Pb together with the charge form factor in nuclear ground states [37,38].

As seen from Fig. 2, the RCNP [14] and TAMU [6] data for ISGMR in ^{154}Sm deviate from each other. Unlike the TAMU data, the RCNP data (i) give a strong tail of the monopole strength above the ISGMR and (ii) do not exhibit the ISGMR splitting with its pronounced low-energy monopole peak, in spite of the fact that ^{154}Sm is strongly prolate. The discrepancy between RCNP and TAMU data is surprising because both groups use (α,α') reaction and exploit similar multipole decomposition techniques to extract the monopole strength [6,14]. This problem was briefly discussed in our previous studies of ISGMR in spherical [28] and deformed nuclei [25]. As mentioned in [28], a possible reason for the discrepancy could be that different incident energies of α-particle beams had been used in TAMU and RCNP experiments, 240 MeV [6] and 386 MeV [14], respectively. Because (α,α') is a peripheral reaction, the TAMU and RCNP experiments may probe different surface slices and thus experience different compression responses. Indeed, the compression response depends on the nuclear density which significantly varies in the surface region. The TAMU and RCNP discrepancy, being yet unresolved, calls for additional measurements and analysis.

Figure 3 shows results for the chain of Cd isotopes. Here we use recent RCNP data [16] for ^{106,110,112,114,116}Cd and TAMU data [17] for ^{116}Cd. The data are obtained for α-particles with incident energies 400 MeV (RCNP) and 240 MeV (TAMU). In the analysis of [16,17], the open-shell Cd isotopes are treated as spherical. However, the experimental data [29] give for these isotopes a modest axial quadrupole deformation which steadily grows from ^{106}Cd ($\beta = 0.173$) to ^{112}Cd ($\beta = 0.186$) and then sharply drops toward ^{114}Cd ($\beta = 0.130$) and ^{116}Cd ($\beta = 0.135$). Note that earlier experiments [39] deliver similar deformations for $^{110-112}$Cd but much larger for ^{114}Cd ($\beta = 0.190$) and ^{116}Cd ($\beta = 0.191$). Anyway, unlike [16,17], it is more relevant to treat Cd isotopes as slightly deformed. As mentioned above, our calculations demonstrate for these nuclei shallow energy surfaces with too weak minima. So, in our analysis of

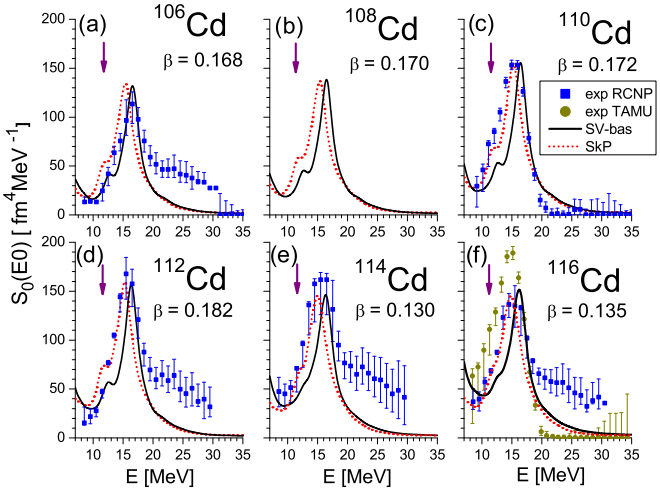

FIG. 3. Isoscalar $E0$ strength functions in Cd isotopes, calculated within QRPA with the forces SV-bas (black solid line) and SkP (red dotted line). For the comparison, the $E0$ data from RCNP [16] (blue filled squares) and TAMU [17] (green filled circles, only for ^{116}Cd) experiments are depicted. The calculated peak energies of the quadrupole branch with $K = 0$ are marked by arrows. The experimental deformation parameters β [29] are indicated for each isotope.

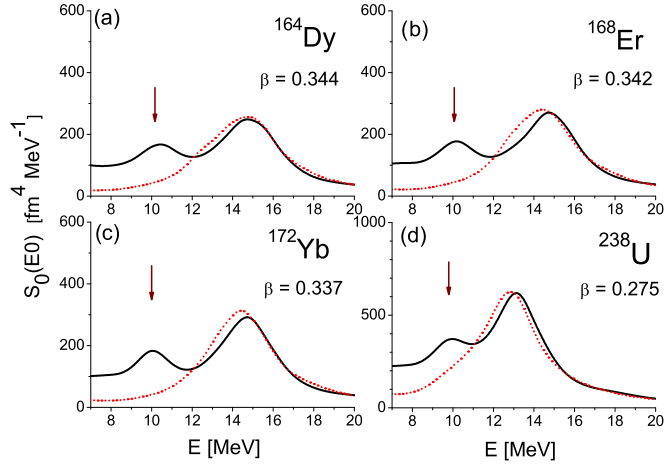

FIG. 4. The QRPA isoscalar $E0$ strength functions in deformed ^{164}Dy, ^{168}Er, ^{172}Yb, and ^{238}U, calculated with (black solid line) and without (red dotted line) the equilibrium deformation (indicated in the plots). The force SV-bas is used. The peak energies of ISGQR($K = 0$) branch are marked by arrows.

ISGMR in $^{106-116}$Cd we use not calculated but experimental deformations [29] given in Fig. 3.

Figure 3 shows that both SV-bas and SkP calculations predict a slight low-energy peak related to the position of the ISGQR($K = 0$) mode. The experimental strength also indicates a slight left shoulder. However, this shoulder is too small and vague to conclude safely on a low-energy peak. So most probable nuclei with $\beta < 0.2$ cannot develop a measurable deformation splitting of ISGMR.

Note that both SV-bas and SkP in general reproduce the energy E_{ISGMR} of the main monopole peak, though the difference between the predictions is 1–2 MeV. SV-bas well describes E_{ISGMR} in ^{106}Cd but somewhat overestimates it in $^{110-116}$Cd while SkP underestimates E_{ISGMR} in ^{106}Cd but performs better in $^{110-116}$Cd. So we meet here again a well-known problem that we do not get a simultaneous good description of ISGMR in different nuclei with one and the same Skyrme force; see, e.g., discussions [3,4,16,28]. However, while in the previous studies doubly magic and open-shell nuclei were compared (with a noticeable compression "softness" in open-shell patterns), here we see a different compression "softness" already between open-shell nuclei. Namely, ISGMR favors a lower K_∞ from SkP in Cd isotopes and larger K_∞ from SV-bas in ^{154}Sm. Mind that the difference in effective mass m_0^*/m does not affect the ISGMR in spherical nuclei [34,35,38] so that K_∞ remains as the only player in this case. But in deformed nuclei there is a combined effect of K_∞ and isoscalar effective mass m_0^*/m. The effective mass can affect ISGQR and thus the $E0$-$E2$ coupling. This in turn can result in a noticeable shift of the main ISGMR peak. As discussed below, in Cd isotopes we get a downshift of the main ISGMR peak (in contrast to well-deformed nuclei which demonstrate a noticeable upshift). Anyway our QRPA analysis of ISGMR in Cd isotopes is still somewhat approximate. A more rigorous treatment should take into account a softness of these nuclei to deformation, possible nonaxiality, and coupling to complex configurations.

For ^{116}Cd, Fig. 3 once more exhibits big deviations between RCNP [16] and TAMU [17] experimental data. The deviations are similar to those for ^{154}Sm: As compared to TAMU, RCNP gives a higher ISGMR energy and a strong strength tail above the resonance. So, RCNP and TAMU deviations have a systematic character and are pertinent to various mass regions. Presently this is a serious obstacle for further progress in ISGMR studies.

In Fig. 4, the ISGMR in strongly deformed nuclei is inspected. Four typical rare-earth and actinide nuclei (^{164}Dy, ^{168}Er, ^{172}Yb, ^{238}U) are considered. The $E0$ strength in these nuclei demonstrates a clear two-peak structure and the low-energy peak originates from the deformation-induced $E0$-$E2$ coupling. In the spherical limit, only the main monopole peak exists. Comparing the strengths in the spherical and deformed cases, one can notice that, in accordance with earlier studies [2,8], the $E0$-$E2$ coupling leads to some upshift of the main ISGMR peak.

In Fig. 5, SV-bas results for ISGMR are shown in ^{242,254,270}No and superheavy ^{264,284,304}Fl($Z = 114$). The No chain includes only deformed isotopes. The larger the isotope deformation, the stronger the low-energy monopole peak. In all these isotopes, the peak energy coincides with the energy of ISGQR($K = 0$) mode. The Fl chain ($Z = 114$) represents isotopes with zero ($A = 304$), modest ($A = 284$), and large ($A = 264$) deformation. The low-energy peak is absent in spherical ^{304}114 but grows from ^{284}114 to ^{264}114. The peak energy matches the ISGQR($K = 0$) energy thus confirming its origin from the $E0$-$E2$ coupling. So superheavy nuclei confirm the physical mechanism of ISGMR splitting pertinent to medium, rare-earth, and actinide nuclei.

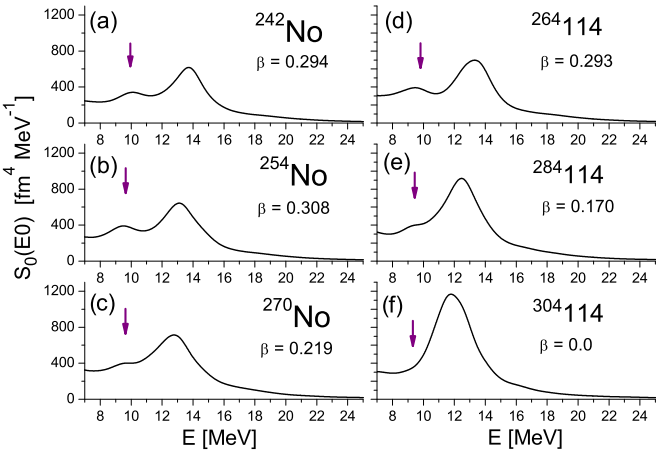

FIG. 5. The QRPA isoscalar $E0$ strength functions for isotopes ^{242,254,270}Nd (left) and ^{264,284,304}114 (right) calculated at equilibrium deformations (indicated in the figure). The force SV-bas is used. The peak energies of ISGQR($K = 0$) branch are marked by arrows.

IV. TRENDS

Our calculations cover a wide mass region $106 < A < 304$ and various deformations $0.17 < \beta < 0.35$. So they are suitable to analyze the trends of the deformation splitting of ISGMR with mass number A and quadrupole deformation β. We do this in terms of the following key features of ISGMR and ISGQR in deformed nuclei.

(1) The peak energy $E_{\rm M}$ of the high-energy (main) ISGMR bump (tending to the principle ISGMR in the spherical limit).
(2) The peak energy $E_{\rm Q}$ of the $K = 0$ branch of ISGQR.
(3) The deformation-induced splitting ΔE_M of the monopole strength (the difference between peak energies of low- and high-energy ISGMR bumps).
(4) The deformation-induced shift dE_M of the high-energy ISGMR bump (the difference between its peak energies computed with and without the deformation).
(5) The fractions S_1 and S_2 of $E0$ strength of low- and high-energy ISGMR bumps.
(6) The widths w_1 and w_2 of the low- and high-energy ISGMR bumps.

The method of calculation of the fractions and widths is described below in discussion of Figs. 9 and 10.

We use for the analysis the nuclei considered above and additionally: ^{148}Nd ($\beta = 0.22$), ^{156}Er ($\beta = 0.215$), ^{160}Er ($\beta = 0.304$), and ^{164}Er ($\beta = 0.337$). Altogether the list of the nuclei covers ^{106,108,110,112,114,116}Cd, ^{142,146,148,150}Nd, ^{154}Sm, ^{164}Dy, ^{156,160,164,168}Er, ^{172}Yb, ^{238}U, ^{242,254,270}No, and ^{264,284,304}Fl. The isotopic chains for medium (Cd), rare-earth (Nd, Er), and superheavy (No, Fl) regions are considered.

A. Model and empirical estimations

The main characteristics of the impact of deformation on the ISGMR were estimated about three decades ago in various models; for a review see [2]. Between them, estimations within the cranking model (CM) [8], variational method (VM) [9], and fluid-dynamical model in the simple scaling approximation (SS) [10] are most often used. SS is self-consistent and based on the simplified Skyrme functional. Here we mainly focus on VM and SS estimates as the most detailed and robust ones. Following [8–10], we consider the estimates in terms of the deformation parameter $\delta = 0.946\beta$. Note that the estimates below concern only energies. We were not able to find any reliable analytical estimates for $E0$ strengths.

In SS [10], the estimates for the observables of our interest read

$$E_{\rm M} \approx E^0_{\rm M}\left[1 - \frac{2}{9}\delta^2 + \frac{4}{9}\gamma_M\delta^2\right] \tag{2a}$$

$$\approx E^0_{\rm M}[1 - 0.22\delta^2 + \underline{1.23\delta^2}] \tag{2b}$$

$$\approx E^0_{\rm M}[1 + 1.01\delta^2], \tag{2c}$$

$$\gamma_{\rm M} = \frac{\left(E^0_{\rm M}\right)^2}{\left(E^0_{\rm M}\right)^2 - \left(E^0_{\rm Q}\right)^2} = 2.777, \tag{2d}$$

$$E_{\rm Q} \approx E^0_{\rm Q}\left[1 - \frac{1}{3}\delta - \frac{1}{18}\delta^2 - \frac{4}{9}\gamma_Q\delta^2\right] \tag{3a}$$

$$\approx E^0_{\rm Q}[1 - 0.33\delta - 0.06\delta^2 - \underline{0.79\delta^2}] \tag{3b}$$

$$\approx E^0_{\rm Q}[1 - 0.33\delta - 0.85\delta^2], \tag{3c}$$

$$\gamma_{\rm Q} = \frac{\left(E^0_{\rm Q}\right)^2}{\left(E^0_{\rm M}\right)^2 - \left(E^0_{\rm Q}\right)^2} = 1.777, \tag{3d}$$

$$dE_{\rm M} \approx E^0_{\rm M}1.01\delta^2, \tag{4}$$

$$\Delta E_{\rm M} \approx E_{\rm M} - E_{\rm Q} \tag{5a}$$

$$\approx E^0_{\rm M}[0.2 + 0.27\delta - 0.18\delta^2 + \underline{1.87\delta^2}] \tag{5b}$$

$$\approx E^0_{\rm M}[0.2 + 0.27\delta + 1.69\delta^2], \tag{5c}$$

where

$$E^0_{\rm M} \approx 80A^{-1/3}{\rm MeV}, \tag{6}$$

$$E^0_{\rm Q} \approx 64A^{-1/3}{\rm MeV} \tag{7}$$

are empirical values for the ISGMR and ISGQR energies in spherical nuclei [2]. The terms with γ_M and γ_Q in Eqs. (2a) and (3a) arise from the $E0$-$E2$ coupling [note the relation $\gamma_{\rm M}/\gamma_{\rm Q} = (E^0_{\rm M}/E^0_{\rm Q})^2$]. In (2b), (3b), and (5b), these terms are underlined to emphasize the impact of coupling. Note that values $\gamma_{\rm M} = 2.777$ and $\gamma_{\rm Q} = 1.777$ are obtained from empirical estimations (6) and (7) (unlike [10] where less realistic values $E^0_{\rm M} \approx 89A^{-1/3}$MeV and $E^0_{\rm Q} \approx 65A^{-1/3}$MeV were implemented).

The VM [9] provides the following estimates:

$$E_{\rm M} = E^0_{\rm M}(1 + 0.86\delta^2), \tag{8}$$

$$E_{\rm Q} = E^0_{\rm Q}(0.93 - 0.27\delta - 0.26\delta^2), \tag{9}$$

$$dE_{\rm M} = E^0_{\rm M}0.86\delta^2, \tag{10}$$

$$\Delta E_{\rm M} = = E^0_{\rm M}(0.26 + 0.22\delta + 1.1\delta^2). \tag{11}$$

For completeness, we quote also the recent empirical systematics [40] for the ISGQR($K = 0$) energy, obtained from self-consistent calculations with Skyrme forces,

$$E_{\rm Q} = E^0_{\rm Q}(1 - 0.240\delta - 0.672\delta^2). \qquad (12)$$

Equations (2a)–(11) show that, despite some modest differences in numerical coefficients, SS and VM lead to similar important qualitative conclusions:

(i) Because of their large numerical coefficients, the δ^2 corrections cannot be omitted. For well-deformed nuclei with $\delta \sim 0.3$, these terms become of the same order of magnitude as the linear δ terms; see (3c), (5c), (9), (11), and (12). Moreover, in (2c), (4), (8), and (10), the terms linear in δ are absent at all and deformation corrections are represented only by the quadratic terms.

(ii) The δ^2 corrections take place even without $E0$-$E2$ coupling. But then their effect is small. The $E0$-$E2$ coupling delivers additional large δ^2 terms which render the δ^2 terms significant.

(iii) Just the $E0$-$E2$ coupling changes the sign and magnitude of the shift $dE_{\rm M}$ as well as the sign and magnitude of the δ^2 contribution to the splitting $\Delta E_{\rm M}$.

(iv) As seen from (5b), the $E0$-$E2$ coupling increases the splitting $\Delta E_{\rm M}$. The same takes place in CM and VM. The result is natural because interaction between two levels always increases the energy distance between them [41].

(v) All deformation corrections in (2a)–(11) include $E^0_{\rm M,Q}$ and so exhibit the mass dependence $A^{-1/3}$.

For a large deformation $\delta = 0.3$, the SS and VM give $dE_{\rm M} = 7.2A^{-1/3}$MeV, $\Delta E_{\rm M} = 34.7A^{-1/3}$MeV and $dE_{\rm M} = 6.2A^{-1/3}$MeV, $\Delta E_{\rm M} = 34.0A^{-1/3}$MeV, respectively. The cranking model [8] gives $\Delta E_{\rm M} = 28.3A^{-1/3}$MeV. So, following these estimates, the deformation effect in ISGMR should be strong. The upshift $dE_{\rm M}$ and deformation splitting $\Delta E_{\rm M}$ can reach 10% and 35%–45% of the resonance energy $E^0_{\rm M}$, respectively. However, as noted in review [2], the estimated splitting significantly exceeds the values from the experiment for ^{154}Sm and schematic QRPA calculations. In this connection, it is interesting to perform a systematic comparison of the estimates with the results of self-consistent QRPA, which is just done below.

B. QRPA trends

In this section, we compare our QRPA results with the estimates given above. Following the notation of Sec. III, we deal here with the deformation parameter β instead of δ.

In Fig. 6, the dependence of the energy $E_{\rm M}$ of the main ISGMR peak on the mass number A is exhibited and compared with the estimate (6). In general the calculated energies are well aligned with the estimate, especially for spherical nuclei ^{142}Nd and ^{304}Fl. However, in deformed nuclei we get $E_{\rm M} < E^0_{\rm M}$ for $A < 150$ and $E_{\rm M} > E^0_{\rm M}$ for $A > 150$. These deviations seem to be caused to a large extent by the deformation-induced shift $dE_{\rm M}$ of the main ISGMR peak. Indeed, as shown below, $dE_{\rm M}$ is negative for Cd isotopes and positive for deformed nuclei

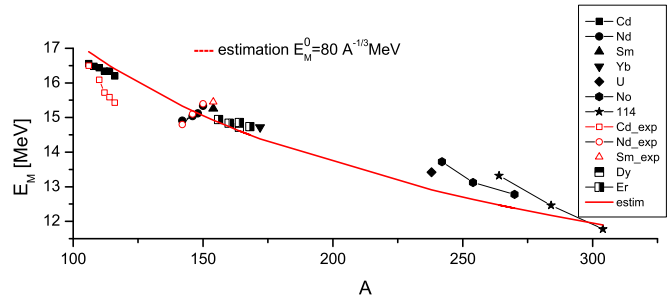

FIG. 6. Dependence of the calculated ISGMR energies (black filled symbols) on the mass number A. For $^{106-116}$Cd, ^{142,146,148}Nd, and ^{154}Sm, the experimental values (red open symbols) are shown. The red line gives the estimate $E^0_{\rm M} \approx 80A^{-1/3}$ MeV.

with $A > 150$, which is in accordance with the deviations. In the isotopic chains for Nd and Er, the deformation and thus $dE_{\rm M}$ grow with A. As a result, $E_{\rm M}$ in Er isotopes decreases with A slower than $\sim A^{-1/3}$. In Nd isotopes, the increase of $dE_{\rm M}$ with A even overrules the trend $\sim A^{-1/3}$ and, as a result, the resonance energy $E_{\rm M}$ grows with A, both in experiment and our calculations. Instead, in No and Fl isotopes the deformation and thus $dE_{\rm M}$ shrinks with A and so these isotopic chains demonstrate even stronger decrease than $\sim A^{-1/3}$. So the shift $dE_{\rm M}$ seems to play a noticeable role in determination of the energy of the main ISGMR peak.

The shift $dE_{\rm M}$ is inspected in detail in Fig. 7. The upper panel shows that it varies between -0.4 and 1.0 MeV, depending on the nucleus and its deformation. What is interesting, $dE_{\rm M}$ for Cd isotopes is negative in contradiction with SS (4) and VM (10) estimates. This signals that SS and VM estimates are not robust for modest deformations $\beta < 0.2$. With the exception of Cd, all other nuclei give positive $dE_{\rm M}$, i.e., an upshift. Its value varies from 0 to 0.6 MeV in rare-earth nuclei to 0.5–1.0 MeV in actinides and superheavy nuclei. So, in contradiction with the estimates, $dE_{\rm M}$ rather increases than

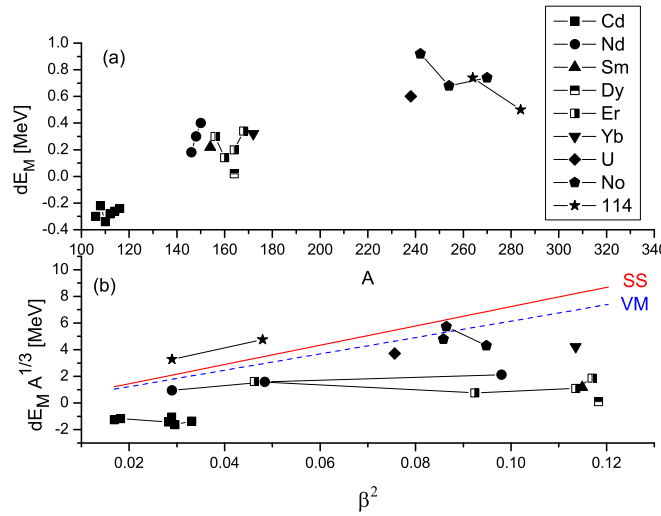

FIG. 7. (a) Dependence of the calculated deformation shift $dE_{\rm M}$ on the mass number A. (b) Dependence of $dE_{\rm M}A^{1/3}$ on the squared deformation parameter β^2. SS (red solid lines) and VM (blue dotted line) estimates are depicted.

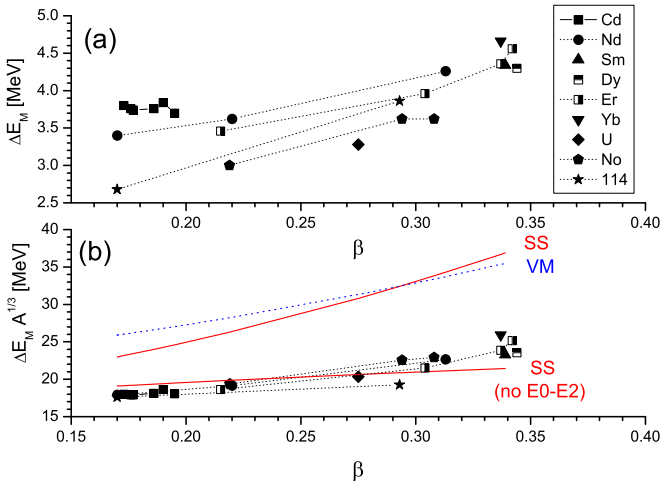

FIG. 8. (a) Dependence of the calculated deformation splitting $\Delta E_{\rm M}$ (black filled symbols) on the deformation parameter β. (b) The same but for $\Delta E_{\rm M} A^{1/3}$. SS estimates (5a)–(5c) and VM estimates (11) are depicted by red solid and blue dotted lines, respectively. For SS, the estimates with (upper line) and without (lower line) $E0$–$E2$ coupling are shown. See more details in the text.

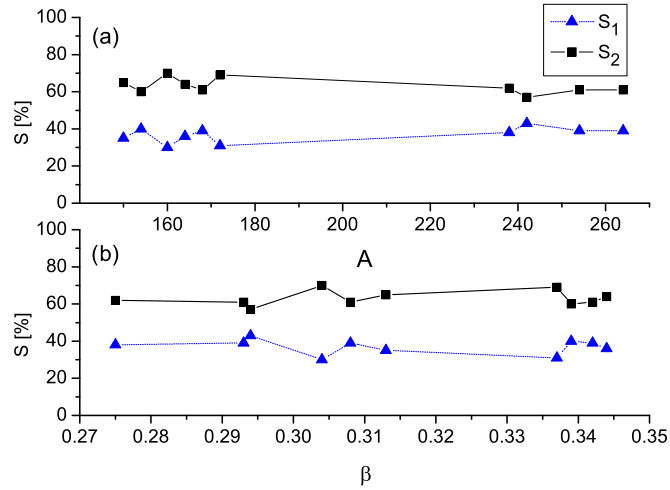

FIG. 9. Calculated fractions S_1 and S_2 (in %) of $E0$ strength in low- and high-energy branches of ISGMR in well-deformed nuclei. The dependence on the mass number (a) and deformation (b) is exhibited.

decreases with A. There are exceptional cases: For example, ^{164}Dy demonstrates a negligible shift $dE_{\rm M} = 0.02$ MeV despite a strong deformation $\beta = 0.344$. So one may state that SS/VM estimates for $dE_{\rm M}$ do not work at a quantitative level.

This is additionally confirmed in the lower panel of Fig. 7 where the values $dE_{\rm M}A^{1/3}$ are depicted. Following the estimates, these values should show a linear dependence on the squared deformation parameter. However, in the chains of Nd and Er isotopes, $dE_{\rm M}A^{1/3}$ are about independent on β^2. For other isotopes, a definite linear dependence on β^2 is also not seen. In addition, the calculations give smaller values of $dE_{\rm M}$ than SS and VM estimates. Only heavy and superheavy nuclei more or less match them. Anyway in rare-earth, actinide, and superheavy regions the calculated $dE_{\rm M}$ is basically large. So this shift has to be taken into account in any analysis of deformation effects in ISGMR.

The splitting $\Delta E_{\rm M}$ of the ISGMR is illustrated in Fig. 8. Both QRPA values as well as SS (5a)–(5c) and VM (11) estimates are given. In QRPA, $\Delta E_{\rm M}$ is determined as the difference between peak energies of the low- and high-energy ISGMR bumps (as is used in experimental data and RPA calculations). Instead, in SS and VM estimates, ΔE is defined as the difference between the ISGMR and ISGQR($K = 0$) energies. The upper panel of Fig. 8 shows that $\Delta E_{\rm M}$ lies in the range 2.5–5 MeV. Especially large $\Delta E_{\rm M}$ is found in ^{174}Yb ($\beta = 0.337$). In ^{154}Sm, the computed splitting 4.34 MeV well agrees with the experimental value 4.12 MeV [6]. The lower panel compares QRPA values of $\Delta E_{\rm M}A^{1/3}$ with SS and VM estimates. The SS data are given with and without $E0$-$E2$ coupling [i.e., with and without the underlined term in Eq. (5b)]. The SS (with the coupling) and VM estimates give similar results and both overshoot QRPA splitting by 20%–35%. This result is in accordance to the earlier finding [2] that observed ISGMR splitting is only two-thirds of the estimates. Only after removing $E0$-$E2$ coupling in SS this estimate comes close to the QRPA values.

Note that this finding should not be treated as an insignificance of $E0$-$E2$ coupling. Instead all our results (spectacular two-bump structure of ISGMR caused by $E0$-$E2$ coupling) testify that the coupling is strong and important. Perhaps Fig. 8 rather indicates that SS overestimates the deformation effect, which gives a false impression that the $E0$-$E2$ coupling is excessive. This is partly confirmed by the comparison of $E_{\rm Q}$ values from the empirical formula (12) and SS analytical estimation (3c): It is seen that (12) gives much smaller deformation correction than (3c).

Because, as compared to SS, QRPA produces a smaller energy difference between the lower and upper ISQMR peaks, it should effectively lead to even stronger coupling between them and to pumping more $E0$ strength into the lower peak. This is demonstrated in Fig. 9, where the calculated relative strengths S_1 and S_2 of the lower and upper ISGMR branches are exhibited. The strengths are obtained by fitting the ISGMR strength function by two Lorentzians at the energy interval 8–18 MeV, embracing both ISGMR branches. To minimize ambiguities, only well deformed nuclei with $\beta > 0.27$ are considered. Because of using a narrow interval $\beta = 0.27$–0.35, the dependence of S_1 and S_2 on β is not so evident. However Fig. 9 allows one to demonstrate typical values of S_1 and S_2 in different mass regions. Remarkably large values of S_1 are obtained for heavy and superheavy nuclei ^{284}Fl ($\beta = 0.170, S_1 = 28\%$), ^{238}U ($\beta = 0.275, S_1 = 38\%$), and ^{242}No ($\beta = 0.294, S_1 = 43\%$). So heavy and superheavy nuclei are promising samples to observe the $E0$-$E2$ coupling. In addition to that, large values of $S_1 \geqslant 35\%$ are obtained in well-deformed rare-earth nuclei ^{150}Nd($\beta = 0.313, S_1 = 35\%$), ^{154}Sm ($\beta = 0.339, S_1 = 40\%$, as compared to the experimental value $32 \pm 2\%$ [6]), ^{164}Dy ($\beta = 0.344, S_1 = 36\%$), and ^{168}Er ($\beta = 0.342, S_1 = 39\%$). In general our calculations for well-deformed nuclei give larger $S_1 \approx 35\%$–40% as compared with $S_1 \approx 20\%$–25% in early estimates [8–10]. As mentioned

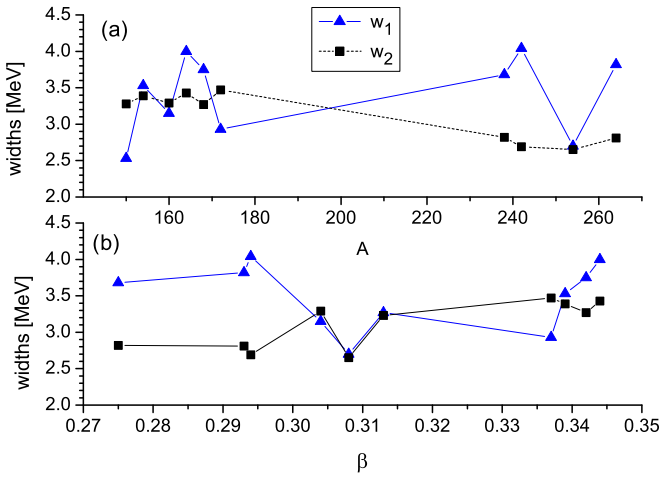

FIG. 10. Calculated widths w_1 and w_1 of lower and upper ISGMR branches in well-deformed nuclei. The dependence on the mass number (a) and deformation (b) is exhibited.

above, this can be caused by a smaller energy distance between the lower and upper ISGMR peaks in our QRPA calculations. At the same time, our results are in reasonable agreement with available experimental data which in average give a higher monopole peak twice stronger than the lower one [2].

Figure 10 shows the calculated widths w_1 and w_2 of the low- and high-energy branches of ISGMR. The widths are also obtained by fitting of the ISGMR strength function by two Lorentzians. And again only nuclei with a large deformation $\beta > 0.27$ are considered. Figure 10 shows that both widths vary in the range 2.5–4 MeV, which is in accordance with the summary in [2]. In average, w_1 and w_2 are of the same order but various ratios $w_1 > , \approx , < w_2$ are realized. Following the bottom panel, there is no definite dependence of the widths on the nuclear deformation. Instead, they fluctuate from nucleus to nucleus and seem to be mainly determined by the actual level structure (spectral fragmentation). The absence of definite dependence on β may be explained by two opposite trends caused by the deformation. On the one hand, the deformation should increase the width of the main ISGMR branch. But, on the other hand, the larger the deformation, the more $E0$ strength is transferred to the low-energy branch, which effectively decreases the width of the main resonance. Note that different ratios w_1/w_2 were also found in the previous study [26] for Nd-Sm isotopes.

V. CONCLUSIONS

The deformation-induced splitting of isoscalar giant monopole resonance (ISGMR) was systematically investigated for a variety of axially deformed nuclei in a wide mass region $106 \leqslant A \leqslant 304$, including medium, rare-earth, actinide, and superheavy nuclei. Altogether 24 nuclei were involved. The analysis was carried out in the framework of the self-consistent quasiparticle random-phase-approximation (QRPA) method based on the Skyrme functional [31]. Some auxiliary calculations were performed with the separable self-consistent QRPA [32,33]. The Skyrme force SV-bas [35] with incompressibility $K_\infty = 234$ MeV and isoscalar effective mass $m_0^*/m = 0.9$ was mainly used, complemented by the results from the Skyrme force SkP$^\delta$ with lower $K_\infty = 202$ MeV and somewhat higher $m_0^*/m = 1$. To the best of our knowledge, this is the first systematic self-consistent study of the deformation-induced splitting of ISGMR, covering nuclei from different mass regions.

The calculations confirmed the earlier result [2] that deformation-induced coupling between monopole and quadrupole excitations leads to the splitting of ISGMR into low- and high-energy branches. The energy of the lower branch coincides with the energy of $K = 0$ part of isoscalar giant quadrupole resonance (ISGQR). This effect was found in all considered deformed nuclei, including superheavy ones.

Following our analysis, the splitting of ISGMR cannot be easily discriminated in nuclei with modest deformation $\beta < 0.2$. In particular, it can hardly be observed in soft Cd isotopes. At the same time, in rare-earth, actinide, and superheavy mass regions there are many well-deformed ($\beta > 0.3$) nuclei where the splitting is strong enough to be observed experimentally. Our calculations well reproduce experimental distributions of the monopole strength in ^{154}Sm [6] and Cd isotopes [16]. However, it should be noted that available experimental data on ISGMR in well-deformed nuclei are still sparse and even contradicting. For example, in well-deformed ^{154}Sm a clear ISGMR splitting takes place in the TAMU experiment [6] but not in the data from RCNP [14]. Our QRPA results agree well with the TAMU data. Anyway, there is a need for further high-accuracy experimental studies. Moreover these studies should cover more of the well-deformed nuclei.

Because our investigation involves nuclei from different mass regions, it allows one to check various systematics, e.g., the trends with the mass number A and deformation β. In this connection, we analyzed and tested early estimates of different characteristics of deformation splitting [9,10]. The qualitative features following from the estimates were generally confirmed. At the same time essential differences at the quantitative level were found. Altogether, our QRPA analysis has revealed the following peculiarities of ISGMR splitting:

(i) The $E0$-$E2$ coupling leads to a noticeable (from -0.4 to 1.0 MeV) energy shift $dE_{\rm M}$ of the main (upper) ISGMR peak. In particular for isotopic chains, this shift can noticeably affect the dependence of the ISGMR energy on mass number. The effect is strong and should be taken into account in any analysis of ISGMR in deformed nuclei. Unlike the estimates [9,10], the shift $dE_{\rm M}$ is negative in Cd isotopes. In other nuclei, it is positive but not proportional to the squared deformation parameter β^2 as was predicted [9,10].

(ii) The QRPA result for the energy splitting $\Delta E_{\rm M}$ of ISGMR is 20%–30% smaller than estimated in simple models [9,10], which is in accordance with earlier conclusions [2]. This has an important consequence: Smaller energy distance between the lower and upper ISGMR peaks results in stronger $E0$-$E2$ coupling and thus in more pumping of $E0$ strength to the lower peak.

(iii) As a result, QRPA predicts in well-deformed nuclei a large fraction of $E0$ strength in the lower peak. This fraction can reach 30%–40% as compared to ∼30% in earlier studies [2] and recent experiment for ^{154}Sm [6]. The large strength of

the lower peak opens promising perspectives for experimental observation of the splitting of ISGMR strength.

(iv) In accordance to recent QRPA study of ISGMR in Nd and Sm isotopes [26], our analysis shows that widths w_1 and w_2 of the lower and upper ISGMR peaks are generally of the same order of magnitude (2.5–4 MeV), although they may exhibit different ratios, depending on the nucleus. It is remarkable that both widths do not demonstrate a definite dependence on the deformation β. This can be explained, at least for the upper peak, by two opposite trends caused by the deformation. On the one hand, the deformation should increase the width of the main upper ISGMR peak (deformation spread). But, on the other hand, the larger the deformation, the more $E0$ strength is transferred to the lower peak, which effectively decreases the width of the main peak.

Finally note that the deformation-induced coupling of the monopole and quadrupole giant resonances is the only example of a strong and measurable coupling between giant resonances. This coupling is of crucial importance when using the ISGMR in deformed nuclei for the exploration of the nuclear incompressibility. Further, the $E0$-$E2$ coupling can be useful for a combined investigation of nuclear incompressibility and isoscalar effective mass [26]. The lower peak of ISGMR could be a useful indicator of the $K = 0$ branch of ISGQR.

The study of the deformation-induced ISGMR splitting in self-consistent models still leaves many open questions. This subject needs both a strong theoretical effort and new high-accuracy experiments for a variety of deformed nuclei.

ACKNOWLEDGMENTS

The work was partly supported by DFG Grant No. RE 322/14-1, Heisenberg-Landau (Germany-BLTP JINR), and Votruba-Blokhincev (Czech Republic-BLTP JINR) grants. P.-G.R. is grateful for the BMBF support under Contracts No. 06 DD 9052D and No. 06 ER 9063. The support of the Czech Science Foundation (P203-13-07117S) is appreciated. A.R. is grateful for support from the Slovak Research and Development Agency under Contract No. APVV-15-0225.

[1] J. Blaizot, Phys. Rep. **64**, 171 (1980).
[2] M. N. Harakeh and A. van der Woude, *Giant Resonances* (Oxford, Clarendon, 2001).
[3] G. Colò, Phys. Part. Nuclei **39**, 286 (2008).
[4] P. Avogadro and C. A. Bertulani, Phys. Rev. C **88**, 044319 (2013).
[5] J. R. Stone, N. J. Stone, and S. A. Moszkowski, Phys. Rev. C **89**, 044316 (2014).
[6] D. H. Youngblood, Y. W. Lui, H. L. Clark, B. John, Y. Tokimoto, and X. Chen, Phys. Rev. C **69**, 034315 (2004).
[7] T. Kishimoto, Phys. Rev. Lett. **35**, 552 (1975).
[8] Y. Abgrall, B. Morand, E. Caurier, and N. Grammaticos, Nucl. Phys. A **346**, 431 (1980).
[9] S. Jang, Nucl. Phys. A **401**, 303 (1983).
[10] S. Nishizaki and K. Ando, Prog. Theor. Phys. **73**, 889 (1985).
[11] D. Zawischa, J. Speth, and D. Pal, Nucl. Phys. A **311**, 445 (1978).
[12] M. Buenerd, D. Lebrun, P. Martin, P. de Saintignon, and C. Perrin, Phys. Rev. Lett. **45**, 1667 (1980).
[13] U. Garg, P. Bogucki, J. D. Bronson, Y. W. Lui, and D. H. Youngblood, Phys. Rev. C **29**, 93 (1984).
[14] M. Itoh, H. Sakaguchi, M. Uchida, T. Ishikawa, T. Kawabata, T. Murakami, H. Takeda, T. Taki, S. Terashima, N. Tsukahara, Y. Yasuda, M. Yosoi, U. Garg, M. Hedden, B. Kharraja, M. Koss, B. K. Nayak, S. Zhu, H. Fujimura, M. Fujiwara, K. Hara, H. P. Yoshida, H. Akimune, M. N. Harakeh, and M. Volkerts, Phys. Rev. C **68**, 064602 (2003).
[15] D. H. Youngblood, Y. W. Lui, Krishichayan, J. Button, M. R. Anders, M. L. Gorelik, M. H. Urin, and S. Shlomo, Phys. Rev. C **88**, 021301(R) (2013).
[16] D. Patel *et al.*, Phys. Lett. B **718**, 447 (2012).
[17] Y. W. Lui, D. H. Youngblood, Y. Tokimoto, H. L. Clark, and B. John, Phys. Rev. C **69**, 034611 (2004).
[18] M. Bender, P.-H. Heenen, and P.-G. Reinhard, Rev. Mod. Phys. **75**, 121 (2003).
[19] D. Vretenar, A. V. Afanasjev, G. A. Lalazissis, and P. Ring, Phys. Rep. **409**, 101 (2005).
[20] S. Péru and H. Goutte, Phys. Rev. C **77**, 044313 (2008).
[21] C. Losa, A. Pastore, T. Dossing, E. Vigezzi, and R. A. Broglia, Phys. Rev. C **81**, 064307 (2010).
[22] Y. K. Gupta, U. Garg, J. T. Matta, D. Patel, T. Peach *et al.*, Phys. Lett. B **748**, 343 (2015).
[23] J. Kvasil, V. O. Nesterenko, A. Repko, P.-G. Reinhard, and W. Kleinig, EPJ Web of Conf. **107**, 05003 (2016).
[24] K. Yoshida, Phys. Rev. C **82**, 034324 (2010).
[25] J. Kvasil, V. O. Nesterenko, A. Repko, D. Bozik, W. Kleinig, and P.-G. Reinhard, J. Phys.: Conf. Series **580**, 012053 (2015).
[26] K. Yoshida and T. Nakatsukasa, Phys. Rev. C **88**, 034309 (2013).
[27] S. Péru, G. Gosselin, M. Martini, M. Dupuis, S. Hilaire, and J.-C. Devaux, Phys. Rev. C **83**, 014314 (2011).
[28] J. Kvasil, D. Božik, A. Repko, P.-G. Reinhard, V. O. Nesterenko, and W. Kleinig, Phys. Scr. **90**, 114007 (2015).
[29] Evaluated Nuclear Structure Data File [http://www.nndc.bnl.gov].
[30] P. Ring and P. Schuck, *Nuclear Many Body Problem*, (Springer-Verlag, New York, 1980).
[31] A. Repko, J. Kvasil, V. O. Nesterenko, and P.-G. Reinhard, arXiv:1510.01248.
[32] V. O. Nesterenko, J. Kvasil, and P.-G. Reinhard, Phys. Rev. C **66**, 044307 (2002).
[33] V. O. Nesterenko, W. Kleinig, J. Kvasil, P. Vesely, P.-G. Reinhard, and D. S. Dolci, Phys. Rev. C **74**, 064306 (2006).
[34] M. Bender, K. Rutz, P.-G. Reinhard, and J. A. Maruhn, Eur. Phys. J. A **8**, 59 (2000).
[35] P. Klupfel, P.-G. Reinhard, T. J. Burvenich, and J. A. Maruhn, Phys. Rev. C **79**, 034310 (2009).
[36] J. Dobaczewski, W. Nazarewicz, T. R. Werner, J.-F. Berger, C. R. Chinn, and J. Dechargé, Phys. Rev. C **53**, 2809 (1996).
[37] J. Erler and P.-G. Reinhard, J. Phys. G **42**, 034026 (2014).
[38] P.-G. Reinhard, Phys. Scr. **91**, 023002 (2015).
[39] S. Raman, C. W. Nestor Jr., and P. Tikkanen, At. Data Nucl. Data Tables **78**, 1 (2001).
[40] G. Scamps and D. Lacroix, Phys. Rev. C **89**, 034314 (2014).
[41] R. F. Casten, *Nuclear Structure from a Simple Perspective* (Oxford University Press, Oxford, 1990).